

A Self-Training Approach for Point-Supervised Object Detection and Counting in Crowds

Yi Wang, *Graduate Student Member, IEEE*, Junhui Hou, *Senior Member, IEEE*, Xinyu Hou, *Student Member, IEEE*, and Lap-Pui Chau, *Fellow, IEEE*

Abstract—In this paper, we propose a novel self-training approach which enables a typical object detector trained only with point-level annotations (i.e., objects are labeled with points) to estimate both the center points and sizes of crowded objects. Specifically, during training we utilize the available point annotations to directly supervise the estimation of the center points of objects. Based on a locally-uniform distribution assumption, we initialize pseudo object sizes from the point-level supervisory information, which are then leveraged to guide the regression of object sizes via a crowdedness-aware loss. Meanwhile, we propose a confidence and order-aware refinement scheme to continuously refine the initial pseudo object sizes such that the ability of the detector is increasingly boosted to simultaneously detect and count objects in crowds. Moreover, to address extremely crowded scenes, we propose an effective decoding method to improve the representation ability of the detector. Experimental results on the WiderFace benchmark show that our approach significantly outperforms state-of-the-art point-supervised methods under both detection and counting tasks, i.e., our method improves the average precision by more than 10% and reduces the counting error by 31.2%. In addition, our method obtains the best results on the dense crowd counting dataset (i.e., ShanghaiTech) and vehicle counting datasets (i.e., CARPK and PUCPR+) when compared with state-of-the-art counting-by-detection methods. We will make the code publicly available to facilitate future research.

Index Terms—Convolutional neural network (CNN), object detection, crowd counting, self-training, weak supervision.

I. INTRODUCTION

With a huge amount of population living in cities, crowd scenes have become a fundamental yet challenging scenario in a wide variety of applications, such as video surveillance [1], crowd analysis [2], [3], and safety monitoring [4], [5]. Objects in dense crowds present small sizes, large scale variations, and high occlusions, which poses great challenges to object detection methods that simultaneously predict the locations and sizes of objects in an image.

The advances of deep neural networks (DNNs) raise an issue of enormous demand for data annotations. It is, however, very costly and laborious to collect object-level bounding box annotations which are usually needed for training DNN-based object detection methods, especially for images containing thousands of objects. Current crowd counting datasets provide only point-level annotations, and usually human heads are



Fig. 1: Illustration of generated training examples at different phases by our self-training approach. The images are from WiderFace dataset [10]. The green dots shown at the centers of faces stand for the point-level annotations. (a): Before training, the pseudo object sizes (red boxes) generated by the proposed locally-uniform distribution assumption. The numbers shown at the top-right corner of red boxes stand for object crowdedness. (b): After training, the refined pseudo object sizes (blue boxes) by our crowdedness-aware loss and the confidence and order-aware refinement scheme. The numbers shown at the top-left corner of blue boxes stand for the posterior probabilities of the pseudo object sizes. *Zoom in the figure for better viewing.*

labeled as the central points, e.g., the green dots shown in Fig. 1. Due to the lack of object sizes, state-of-the-art DNN-based generic object detectors [6] cannot be trivially applied to such point supervision. As pioneers, Liu *et al.* [7] introduced a pseudo size updating scheme in a detection network to estimate object sizes. Sam *et al.* [8] proposed an LSC-CNN to achieve higher detection performance in crowd scenes. However, these works are still not on par with box-supervised methods (e.g., Faster R-CNN [9]) in the detection task. As for the counting task, these methods, denoted as counting-by-detection methods, can count objects by filtering out low-confidence objects with a threshold. However, they also suffer from crowded objects in the counting task.

Alternatively, recent crowd counting methods [11]–[13], named counting-by-regression methods, bypass the locations and sizes of objects but employ DNNs to regress a density map

Yi Wang, Xinyu Hou, and Lap-Pui Chau are with School of Electrical and Electronics Engineering, Nanyang Technological University, Singapore, 639798 (e-mail: {wang1241, hou0008}@e.ntu.edu.sg, elpchau@ntu.edu.sg).

Junhui Hou is with the Department of Computer Science, City University of Hong Kong (e-mail: jh.hou@cityu.edu.hk).

Corresponding author: Lap-Pui Chau.

which is further integrated to obtain the overall count. These methods have achieved outstanding counting performance in dense crowds. However, they only aim to count the number of objects and lose individual information, i.e., the location and size of each object instance. We argue that the density map only contains weak information about the crowds, while locations and sizes of object instances provide much more important information for other computer vision applications, such as multi-object tracking [14], [15], face recognition [10], [16], and person re-identification [17].

In view of these issues, we propose a novel self-training approach, which is capable of training a typical detection method only with point-level annotations such that it can accurately and simultaneously detect and count the objects in dense crowds. Specifically, based on a keypoint-based detector, i.e., center and scale prediction (CSP) [18], we decouple detection as the separate estimation of the center points and sizes of objects. The estimation of the center points are directly supervised by the known point-level annotations during training. As the ground-truth object sizes are not accessible, we propose a simple yet effective assumption in crowd scenes, called locally-uniform distribution assumption (LUDA), to generate the initial pseudo size for each object (see the red bounding boxes shown in Fig. 1(a)). Meanwhile, we propose a crowdedness-aware loss to emphasize the contributions of crowded objects in object size regression (see the crowdedness at the top-left corner of red boxes in Fig. 1(a)). Moreover, we propose a confidence and order-aware refinement scheme to continuously update the pseudo sizes during training, which performs the refinement operation by considering both the prior confidences and the updating order of pseudo sizes, such that the detection ability of the detector is increasingly boosted (see the blue bounding boxes shown in Fig. 1(b) for the refined pseudo object sizes). In addition, to deal with highly dense crowds (e.g., one person represented by several pixels in an image on the ShanghaiTech [19] dataset), we propose an effective decoding method to improve the representation ability of the CSP detector, in which a feature fusion and decoding technique is employed to restore the full-resolution feature maps.

Extensive experimental results show that our approach outperform start-of-the-art point-supervised methods to a significant extent in terms of the detection performance, i.e., more than 10% AP improvement is achieved. Moreover, our method even produces comparable performance to the box-supervised Faster R-CNN on the WiderFace benchmark [10]. On dense crowd datasets, e.g., ShanghaiTech [19], our method produces the best results among state-of-the-art counting-by-detection methods and obtains comparable results when compared with latest counting-by-regression methods. Note that the bounding boxes produced by our method are more meaningful than the density map produced by counting-by-regression methods.

The rest of this paper is organized as follows. In Section II, we introduce the related work on object detection and counting in dense crowds. Then, the proposed method is presented in detail in Section III. Experimental results and ablation studies are provided in Section IV. Finally, we conclude this paper in Section V.

II. RELATED WORK

A. Object Detection in Dense Crowds

Benefiting from the advances of DNNs, recent object detectors, such as Faster R-CNN [9], RetinaNet [20], and CenterNet [21], achieve appealing performance. Despite the remarkable progress made, these methods encounter difficulties when counting small and heavily occluded objects in crowded scenes. To enhance the detectors' abilities, Liu *et al.* [18] proposed a keypoint-based detector named CSP to predict the central points and scale of objects separately. Goldman *et al.* [22] presented a deep-learning-based method for precise object detection in densely packed scenes. They introduced a soft intersection-over-union (IoU) network layer and an expectation-maximization (EM) based clustering method to deal with overlapped objects in the dense scenes. Though these above detectors all achieve good performance, they have to be trained and supervised by box-annotated examples.

Most crowd counting datasets only provide point annotations for denser crowds. It is nontrivial to train a detector with the point supervision. Recently, several works begin to use the blobs [23] to localize the individuals in crowds, and even to estimate the sizes of the heads [7], [8], with only point-level annotations. Laradji *et al.* [23] argued that the unnecessary size and shape information drags the performance of detection-based methods in counting problems. A localization-based counting loss that combines image-level, point-level, split-level, and false-positive loss is used to train a fully convolutional network (FCN) such that it could produce the blobs in the center of objects. Based on a regression-based network, Idrees *et al.* [24] proposed a post-processing method to find the local peaks on the density map as the center locations of heads. As a baseline method, Sam *et al.* [8] applied a threshold technique on the density map of the CSRNet [11] to obtain detections (called CSR-A-thr). However, these methods only localize the center points of individuals in crowds.

To further estimate the sizes of individuals, Liu *et al.* [7] proposed a detection network, named PSDDN, which builds a strong baseline for point-supervised detection and counting in crowds. The PSDDN employs the nearest neighbor distance [19] to initialize the pseudo boxes, and updates the pseudo boxes by choosing smaller box predictions. Another state-of-the-art method, named LSC-CNN, was proposed recently by Sam *et al.* [8], where the objective is to locate, size, and count every person in crowds. The detection methods can be directly used to count objects [8] since the number of detections is also the count of objects.

B. Object Counting in Dense Crowds

Bypassing localization, counting-by-regression methods [1], [19], [25], [26] have been proposed to address the crowd counting problems and have dominated crowd counting for years. Instead of directly regressing the global count adopted in early works [4], [27], current approaches [11], [12], [28] exploit DNNs to estimate the density map [29], where the count is obtained via the integral over the map. Training this kind of network is to build a mapping between an image and a density map. A multi-column structure [19], [25] was

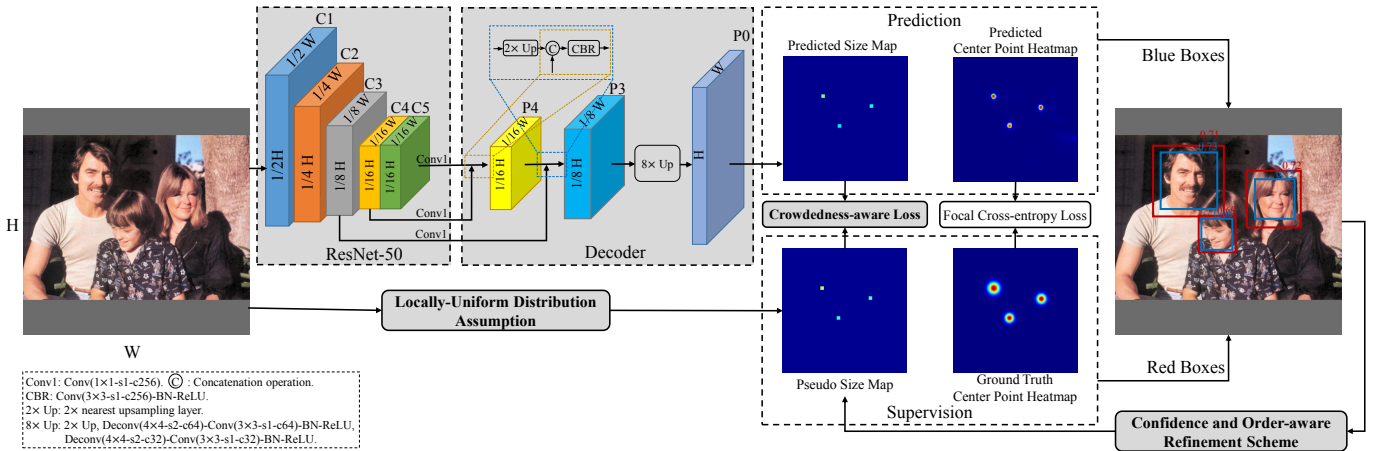


Fig. 2: Illustration of the proposed self-training framework for training a detector only with point-wise supervision. The decoder produces high-resolution feature maps for the estimation of center points and sizes of objects. Before training, the pseudo object sizes are first generated from the point-wise supervisory information, based on our locally-uniform distribution assumption. During training, the pseudo object sizes are further refined by our confidence and order-aware refinement scheme under the supervision of the proposed crowdedness-aware loss. Here an image with sparse objects is used for clear visualization purposes.

introduced to learn the multi-scale features for representing large scale variation of objects. Li *et al.* [11] demonstrated the redundancy of features in the multi-column structure and proposed a single-column deep structure (e.g., VGG [30]) with dilated convolution layers, which achieved better results. Cao *et al.* [28] proposed a scale aggregation module to learn the scale diversity of features. Shi *et al.* [12] repurposed point annotations as a segmentation map and a global density map. By exploiting attention mechanisms, Sindagi *et al.* [31] proposed an attention-based crowd counting network (HACCN) to enhance the different-level features of the network. A recent survey paper written by Gao *et al.* [13] reviews over two-hundred crowd counting works, showing the improvement in this filed.

Despite the counting-by-regression methods obtain state-of-the-art counting performance, they sacrifice the location and size information of objects [13]. We argue that the count is rough information for the crowds and not enough for further use of high-level vision tasks. In our work, we count objects by our object detections.

C. Counting from Drone View

Another dense case appears in vehicle counting from drone images. Hsieh *et al.* [32] introduced a large-scale car parking lot dataset (CAPPK), which consists of approximately 90k cars. Motivated by the regular spatial layout of cars, they proposed a layout proposal networks (LPN) to count vehicles. Without local annotations such as bounding boxes or points, Stahl *et al.* [33] proposed a general object counting method that uses local image regions to predict the global image-level counts. Goldman *et al.* [22] considered that vehicles in drone images are a densely packed scene. Therefore, they used their object detection method in this scenario. To deal with the failure of state-of-the-art detectors in drone scenes, Li *et al.* [34] made a set of modifications for detection. An effective loss is proposed to yield the scale-adaptive anchors.

Then, the circular flow is applied to guide feature extraction. Third, a counting regularized constraint is introduced to the loss function. For drone-view datasets [32], we will compare our method with them in Sect. IV-C.

III. PROPOSED METHOD

Fig. 2 illustrates the proposed self-training framework, which is capable of training a typical object detector only with point-level annotations for simultaneous object detection and counting. The framework is built on an anchor-free keypoint-based object detector, i.e., CSP detector [18]. To be specific, a locally-uniform distribution assumption is proposed to generate the initial pseudo size for each object, and a crowdedness-aware loss is proposed to emphasize the pseudo sizes of crowded objects in size regression. Furthermore, a confidence and order-aware refinement scheme is proposed to update the pseudo sizes in each training iteration. In addition, a decoding method is proposed to handle dense crowds. In what follows, we first present the detection network and then the proposed self-training approach in detail.

A. Detection Network

We employ the keypoint-based detection method because it allows to separately estimate the center point and size of objects. Therefore, the center points could be directly supervised by the point-level annotation, while the size estimation is accomplished by the proposed modules. In addition, it is anchor box-free.

1) *Architecture*: For the datasets with medium-density crowds (e.g., WideFace [10], CARPK and PUCPR+ [32]), we employ the original network in [18]. For the dataset with high-density crowds (e.g., ShanghaiTech [19]), however, the original network performs poorly since the center point prediction fails to represent highly dense objects in its output feature map of size $\frac{H}{4} \times \frac{W}{4}$, where H and W are the height

and width of the input image, respectively. Hence, we propose an effective decoding method to handle this issue.

As illustrated in Fig. 2, the detection network contained in our approach adopts the five-stage ResNet-50 [35] as the backbone network, where each stage downsamples the feature maps by a factor of 2, except for Stage-5 that uses the dilated convolutions to keep the stride the same as Stage-4. Let $C_i, i \in \{1, 2, \dots, 5\}$ be the output feature maps of the i -th stage. In the *Decoder*, three Conv(1×1-s1-c256) are applied to reduce the number of channels of C_5 , C_4 , and C_3 , where Conv denotes the convolutional layer, and (1×1-s1-c256) means the layer with the kernel of 1×1, the stride of 1, and the channel of 256. Then, we employ a top-down feature fusion manner to merge C_5 , C_4 , and C_3 , generating the fused features P_3 . The fusion manners are shown as the dotted yellow and blue rectangle in Fig. 2. Finally, we use an $8 \times$ Up structure to decode the fused features, which consists of a $2 \times$ nearest upsampling layer followed by two Deconv(4×4-s2)-Conv(3×3-s1)-BN-ReLU, where Deconv, BN, and ReLU denote the deconvolution, batch normalization, rectified linear unit, respectively. The decoder produces the output feature maps (P_0) with the same size as the input, i.e., $H \times W$. There are two separate heads (i.e., Conv(1×1-s1-c1)) for center point and size prediction, producing the center point heatmap and the size map.

2) *Supervision information*: Let $\{\mathbf{p}_j\}_{j=1}^M$ be the point-wise annotations, where $p_j := (x_j, y_j)$ is the 2D coordinates of the center of the j -th object in an image, and M is the total number of objects in an image. As shown in Fig. 2, to supervise the estimation of object center points, we generate a ground-truth center point heatmap $Q \in [0, 1]^{H \times W}$ with 1 for objects' center points and 0 for negative points. To decrease the ambiguity of negative points surrounding the positive ones, we place a normalized 2D Gaussian mask at the center location of each positive point, as performed in [18]. If two masks overlap, we choose the element-wise maximum for the overlapped region. For the object size supervision, we generate pseudo object sizes denoted by s_j , which will be introduced in Sec. III-B. Here we assume that the objects (e.g., heads and faces) have an aspect ratio of 1 in crowded scenes. We assign $\log(s_j)$ to the j -th object's center coordinates (x_j, y_j) and zeros to other locations, generating the size map $S \in \mathbb{R}^{H \times W}$. For the original CSP with the output of size $\frac{H}{4} \times \frac{W}{4}$, an offset map is appended to estimate the discretization error caused by the stride of 4. The ground-truth offset for p_j is defined as $\frac{x_j}{4} - \lfloor \frac{x_j}{4} \rfloor$ and $\frac{y_j}{4} - \lfloor \frac{y_j}{4} \rfloor$ on the x -axis and y -axis, respectively, which is assigned to (x_j, y_j) on the offset map. $\lfloor r \rfloor : \mathbb{R} \rightarrow \mathbb{Z}$ of a real number r denotes the greatest integer less than or equal to r .

3) *Loss function*: We apply the focal cross-entropy loss [18], [21] to each pixel on the center point heatmap:

$$L_c = -\frac{1}{M} \sum_{j=1}^M \begin{cases} (1 - \hat{q}_j)^\gamma \log(\hat{q}_j), & \text{if } q = 1, \\ A(1 - q_j)^\delta (\hat{q}_j)^\gamma \log(1 - \hat{q}_j), & \text{otherwise,} \end{cases} \quad (1)$$

where \hat{q}_j and q_j are the prediction and the ground truth, respectively; γ is the hyper-parameter of the focal loss [20] which is set to 2 in all experiments; δ is the hyper-parameter

to control the penalty of negatives, which is set to 4 in all experiments; A is the coefficient to address the imbalance between positive and negative points, which is set to 1 (resp. 1/16) for the original CSP (resp. the proposed decoding structure) in all experiments. Intuitively, if we enlarge the CSP's output map by the decoding method from $\frac{H}{4} \times \frac{W}{4}$ to $H \times W$, the number of negative points will increase by 16 times. Hence, we set $A = 1/16$ to balance the positive and negative points. For object size regression, we propose a crowdedness-aware loss $L_{size-\alpha}$, of which the details will be described in Sec. III-C. For offset estimation, the smooth L1 loss [36] is calculated between the ground-truth offsets and predicted ones, denoted as L_o . The overall training objective is

$$L = \lambda L_c + L_{size-\alpha} + L_o, \quad (2)$$

where λ is the weight for center point classification, which is experimentally set to 0.1.

4) *Inference*: The detector first performs a forward pass to generate the center point heatmap, the size map, and the offset map (if it is used). The peak keypoints in the center point heatmap are extracted by a 3×3 max pooling operation. Then, we obtain the center point coordinates of objects whose probabilities are larger than a predefined confidence. The object sizes are obtained from the corresponding coordinates in the size map (see the "Prediction" in Fig. 2). If the offset map is appended, the corresponding offsets are added to object coordinates. Finally, the bounding boxes can be decoded by the coordinates and sizes.

B. LUDA-based Pseudo Object Size Generation

As the ground-truth object sizes are unavailable, we generate pseudo object sizes from the point-wise supervisory information to train the detector. In crowded scenarios, object instances, e.g., heads, faces, or cars, are usually uniformly distributed in an image. According to the geometry-adaptive kernel [19], the size of a typical object is proportional to the distance to its nearest neighbors in dense crowds. This assumption is relatively weak as the objects are not always dense enough in an image. In this paper, we employ the non-uniform kernel [12] to locally restrict the above assumption, and propose the locally-uniform distribution assumption (LUDA). That is, 1) the objects in crowd scenarios are uniformly distributed in a local region and have a similar size in that region; and 2) the crowdedness of the region affects the precision of size estimates. In what follows, we detail our pseudo object size generation method based on LUDA.

Following [12], [19], we first calculate the initial object size of point \mathbf{p}_j according to the distances to its K nearest points, i.e.,

$$\bar{d}_j = \frac{1}{K} \sum_{k=1}^K \beta d_{j,k}, \quad (3)$$

where \bar{d}_j is the initial object size of \mathbf{p}_j , $d_{j,k}$ is the distance between point \mathbf{p}_j and its k -th nearest neighbor, and β is a scalar. The initial object size is further smoothed to reduce

the variation in a local region, leading to the pseudo object size s_j :

$$s_j = \frac{1}{|R_{p_j}|} \sum_{l \in R_{p_j}} \bar{d}_l, \quad (4)$$

where R_{p_j} is the p_j -centered local region, $|R_{p_j}|$ is the number of the points inside R_{p_j} , and \bar{d}_l is the initial size of the l -th point contained in R_{p_j} . We set the R_{p_j} to a circular region so that KD-Tree can be used to improve the calculation speed. $|R_{p_j}|$ affects the precision of size estimates, which will be exploited for the crowdedness-aware loss in Sec. III-C.

Since the crowdedness differs from regions to regions, a single set of parameters in Eqs. (3) and (4) can only fit a specific crowdedness. In experiments, we choose multiple sets of parameters intuitively for different training sets such that the crowded objects have precise pseudo sizes. The detailed parameter settings will be explained in Sec. IV-A.

C. Crowdedness-aware Loss for Object Size Regression

With the pseudo object size s_j , a straightforward way to supervise the regression of object sizes is using the smooth L1 loss [36], i.e.,

$$L_s = \frac{1}{M} \sum_{j=1}^M \text{SmoothL1}(\hat{s}_j, s_j), \quad (5)$$

where \hat{s}_j is the size prediction of the j -th object. However, there is an obvious drawback for Eq. (5), i.e., all object instances equally contribute to the loss, and if some pseudo object sizes are inaccurate (i.e., noisy supervision), the training of the detector will be adversely affected. Moreover, inaccurate pseudo sizes are inevitable since the simple LUDA cannot resolve the complexity of crowded scenes (see Fig. 1(a)). Such a drawback is experimentally verified in the following Table III (see the 5-th entry of Table III).

To this end, we propose a crowdedness-aware loss associating each object instance with its crowdedness, which indicates the importance in object size regression. We formulate the crowdedness-aware loss as

$$L_{size-\alpha} = \frac{1}{M} \sum_{j=1}^M \alpha_j \text{SmoothL1}(\hat{s}_j - s_j), \quad (6)$$

where $\alpha_j \in [0, +\infty)$ is the crowdedness-aware factor controlling weight of the s_j . Based on LUDA, crowded objects can produce more accurate pseudo object sizes than sparse ones, and thus the crowded objects should be assigned with larger weights. Specifically, we define the α_j as an exponential function of the number of objects (crowdedness) inside the local region R_{p_j} , i.e.,

$$\alpha_j = (|R_{p_j}|)^\eta. \quad (7)$$

Here, we use a tunable parameter $\eta \geq 0$ to scale the factor. In practice, we use a threshold to limit the maximum value of α_j to avoid gradient explosion. By assigning crowdedness-aware factors to the pseudo sizes, the loss function emphasizes the influence of the crowded objects and weakens that of the sparse ones. The crowdedness-aware loss enhances the robustness of training on the noisy pseudo sizes.

Algorithm 1 Confidence and Order-aware Refinement Scheme.

Input: The i -th input image X_i with pseudo bounding boxes $B_i = \{b_1, \dots, b_{M_i}\}$, and prior probabilities of the boxes $P(b_j), j \in \{1, \dots, M_i\}$.

Output: Refined pseudo bounding boxes $\tilde{B}_i = \{\tilde{b}_1, \dots, \tilde{b}_{M_i}\}$, and refined prior probabilities $P(\tilde{b}_j)$.

- 1: Forward passing the detector to generate the detections $\hat{B}_i = \{\hat{b}_1, \dots, \hat{b}_{M_i}\}$ with the posterior probabilities $P(C, \hat{B}_i | X_i)$.
 - 2: **for** j in $\{1, \dots, M_i\}$ **do**
 - 3: **if** $P(C, \hat{b}_j | X_i) > P(b_j)$ **then**
 - 4: $P(\tilde{b}_j) \leftarrow P(C, \hat{b}_j | X_i)$
 - 5: $\tilde{b}_j \leftarrow \hat{b}_j$
 - 6: **else**
 - 7: $P(\tilde{b}_j) \leftarrow P(b_j)$
 - 8: $\tilde{b}_j \leftarrow b_j$
-

D. Confidence and Order-aware Refinement Scheme for Pseudo Size Updating

Despite the crowdedness-aware loss is able to boost the robustness of the detector when trained on noisy pseudo sizes, the inaccurate sizes still exist and will affect the backward pass of training. Thus, in this subsection we propose a confidence and order-aware refinement scheme to update pseudo object sizes for better training the detector. In [7], the pseudo bounding boxes are updated by selecting the predicted boxes with the highest scores among those whose sizes are smaller than the pseudo ones. However, such a criterion may not be true in practice since it ignores the following two key issues, resulting in the inaccurate refinement and unstable training process. 1) The prior information. It updates the pseudo sizes without considering their prior confidences. 2) The updating order. All pseudo sizes are treated identically, resulting in the synchronous updating of both accurate and inaccurate sizes.

Instead, by taking prior information into account, we assign every pseudo size with a prior probability at the beginning of training, and if and only if the predicted posterior probability of the detector is larger than the prior probability, we update the pseudo size (resp. prior probability) with the predicted size (resp. posterior probability) for the next epoch. Referring to the prior confidence, our refinement scheme guarantees the detector is trained on increasingly confident examples. Meanwhile, it can update the most inaccurate sizes first, then followed by updating the relatively accurate ones. This is achieved by setting the same prior probability for all pseudo sizes before training. During training, easy examples (e.g., sparse and large objects) with noisy size supervision that achieve high posterior probabilities rapidly are updated first. Then, hard examples (e.g., crowded and small objects) with more accurate size supervision are updated. In other words, the updating order is from noisy sizes to noiseless sizes. The proposed refinement scheme presents a more powerful error-correcting capability than the one in [7]. See the experimental results in Table III.

More specifically, let $b_j = \{p_j, s_j\}$ be a pseudo bounding box centered at p_j with the pseudo size s_j , and the prior probability $P(b_j)$ is assigned to b_j . The object detection problem is cast as learning the posterior $P(C, B | X)$, where

X is the input image, B is the bounding boxes of objects, and $C \in \{0, 1\}$ is the binary class with 0 for background and 1 for object instance. Our refinement scheme, which is merged into the training process, is summarized in Algorithm 1. In each training iteration, after executing a forward path, we obtain the predicted detections \hat{B}_i with the posterior $P(C, \hat{B}_i | X_i)$ (i.e., Line 1). For each instance $j \in \{1, \dots, M_i\}$, if $P(C, \hat{b}_j | X_i)$ is larger than $P(b_j)$, we update the prior probabilities $P(b_j)$ with the posterior $P(C, \hat{b}_j | X_i)$, and update the pseudo bounding boxes \tilde{b}_j with the prediction \hat{b}_j (i.e., Lines 3-5). Otherwise, the prior probability and pseudo bounding box remain unchanged (i.e. Lines 7 and 8). A constant prior probability of 0.6 is assigned to all $\{B_i\}_i^N$ at the beginning of training, where N is the number of training images.

Remark. Here we provide more explanations why our self-training approach enables the detector to update the pseudo size towards the correct direction. The main reasons come from two aspects. First, as analyzed in Sec. III-B, our LUDA-based pseudo size generation method ensures that the pseudo sizes of crowded objects (i.e., hard examples) are more accurate than those of sparse objects. Also, it is known that hard examples have a heavy influence on the detector’s training than easy examples [37], [38]. Thus, when incorporated with the crowdedness-aware loss, the larger number of relatively accurate hard examples in crowded scenes dominate the detector, making it robust to the outliers (e.g., inaccurate pseudo sizes). Second, the pseudo sizes are updated in a robust and orderly manner by our refinement scheme. We set the same initial prior probability for all pseudo bounding boxes. The posterior probability of easy examples will first meet the initial prior probability during training, and thus Algorithm 1 begins with updating the pseudo sizes of inaccurate easy examples. With increasingly accurate easy examples, the detector becomes stronger such that hard examples are then refined. More experimental results to illustrate the effectiveness of the proposed method can be found in Sec. IV-B.

IV. EXPERIMENTAL RESULTS

In this section, we first describe the experiment settings, including datasets, implementation details, and evaluation metrics, followed by ablation studies for verifying the effectiveness of each component of our approach. Finally, we compare our approach with state-of-the-art methods in terms of both detection and counting tasks.

A. Experiment Settings

1) *Datasets:* We used four representative datasets in crowd scenes, i.e., WiderFace [10] for dense face detection, ShanghaiTech [19] for dense crowd counting, and CARPK and PUCPR+ [32] for vehicle counting from the drone view.

WiderFace is one of the most challenging face detection benchmarks, where the 32,203 images containing 393,703 human-labeled faces were captured in a wide variety of imaging conditions, such as large variations in scale and pose, high occlusion, and changeable illumination conditions. 40%, 10%, and 50% of the images were used for training,

TABLE I: The parameter settings of LUDA-based pseudo size generation method for different datasets. “-” means the parameter is not required.

Dataset	Generation Parameters		
	K of Eq. (3)	β of Eq. (3)	Max α_j of Eq. (7)
WiderFace [10]	2	0.5	-
SHA [19]	2	1	50
SHA [19]	2	0.5	50
CARPK [32]	1	1.3	-
PUCPR+ [32]	1	1.2	-

validation, and testing, respectively. Following existing point-supervised detection methods [7], [8], we trained our model on the training set, and reported detection and counting results on the validation set. **ShanghaiTech** presents high-density crowds, which contains 482 images on Part_A (SHA) and 716 images on Part_B (SHB). The number of people in an image ranges from 33 to 3139 on SHA, and 9 to 578 on SHB. We followed the training and testing split in [19] to evaluate the counting and central point localization performance. **CARPK** and **PUCPR+** are composed of images of parking lots from the drone view and high-rise buildings, respectively. **CARPK** contains nearly 90k cars, while **PUCPR+** contains about 17k cars in total. We used the evaluation protocol in their benchmark to evaluate the counting performance of our method.

2) *Implementation details:* The backbone, ResNet-50, was initialized with the pre-trained ImageNet [39] model. We trained our detector on 3 GPUs with the batch size of 12. We adopted Adam [40] optimizer with the learning rate of 7.5×10^{-6} for the WiderFace dataset and 7.5×10^{-5} for the remaining ones. The input images were randomly re-scaled, color distorted, flipped, and then cropped into 704×704 image patches. We used the same re-scale technique as CSP [18]. All training processes can only access to the point annotations. For the datasets with bounding box annotations, i.e., WiderFace, CARPK, and PUCPR+, we calculated their center points for training. We stopped training at 200k, 8k, 45k, and 4.5k iterations for WiderFace, ShanghaiTech, CARPK, and PUCPR+, respectively. Like [7], [18], we performed the multi-scale testing to generate bounding boxes. Then, non-maximum suppression (NMS) was used to filter the generated boxes. Following [8], for the ShanghaiTech dataset, we randomly took 10% training images as validation and chose the best model by performing a threshold search to minimize the counting error on the validation set. The other datasets adopted the confidence threshold of 0.4 to produce boxes for counting.

As mentioned in Sect. III-B, we experimentally chose multiple sets of parameters by which the precise pseudo sizes were generated for crowded objects on training sets. Table I shows the parameter settings used in Eqs. (3) and (7) for different datasets. We especially set the maximum value of α_j to 50 to avoid large gradients since dense crowds of ShanghaiTech produce large values of α_j . For all datasets, we set $\eta = 1$ in Eq. (7).

3) *Evaluation metrics:* For the detection task, we adopted the evaluation protocol in WiderFace [10] to calculate average precision (AP). The true positive is defined as the intersection of union (IoU) between ground truth boxes and detected

TABLE II: Comparisons of our LUDA-based pseudo size generation method with the GAK-based method on the training set of WiderFace [10]. Refinement of pseudo object sizes by our self-training approach is listed at the list entry. The number in the parentheses denotes the IoU threshold for AP calculation. The larger the value of AP is, the better.

Size Generation	AP (0.3)	AP (0.5)	AP (0.7)
GAK [7]	55.8	29.5	7.0
LUDA (ours)	60.3	31.2	7.5
Refined size (ours)	79.4	50.6	14.4

boxes greater than a threshold of 0.5. For the counting task, we adopted the commonly-used mean absolute error (MAE) and root mean square error (RMSE) to evaluate the distance between the predicted counts and the ground-truth ones. The MAE indicates the accuracy of methods, while the RMSE reflects their robustness. They are defined as

$$\text{MAE} = \frac{1}{N_t} \sum_{N_t} |\hat{c}_i - c_i|, \text{RMSE} = \sqrt{\frac{1}{N_t} \sum_{N_t} (\hat{c}_i - c_i)^2}, \quad (8)$$

where N_t is the total number of testing images, and \hat{c}_i and c_i are the estimated count and ground-truth count of the i -th image, respectively. When counting on WiderFace, we used a normalized MAE (NMAE) [12], which normalizes the absolute error by the ground-truth face count.

For the center point localization task, we adopted two evaluation metrics, i.e., AP and mean localization error (MLE) respectively from [7] and [8]. AP defines true positive center point as those whose distance to its ground truth is smaller than a threshold of 20 pixels. MLE calculates the distances in pixels between the predicted center points and their ground truth, and then averages the distances over the testing set. One-to-one matching associates the predictions and the ground truth. In MLE, the false positives and false negatives were assigned with a fixed penalty of 16 pixels. The lower the value of MLE is, the better. The AP and MLE are suitable and reasonable for crowd counting datasets without bounding-box annotations, e.g., ShanghaiTech dataset. These metrics evaluate the localization ability of detection-based algorithms in crowd environments.

B. Ablation Study

We conducted ablation studies on the WiderFace [10] benchmark to evaluate and analyze the improvement of several important modules of our approach, including the locally-uniform distribution assumption (LUDA), the crowdedness-aware loss, and the confidence and order-aware refinement scheme. We evaluated our approach on both the detection and counting tasks. Table II shows the AP results of pseudo size generation methods on the training set of WiderFace, while Table III shows the AP, MAE, and NMAE results on the validation set of WiderFace. The results of state-of-the-art point-supervised detection method (i.e., PSDDN [7]) and the crowd counting method (i.e., Shi *et al.* [12]) are respectively shown in the 1st and 2nd entries of Table III for comparison.

1) *Effectiveness of the pseudo object size generation method:* We compared the proposed LUDA-based pseudo size generation method with the geometry-adaptive kernel (GAK) based method in [7], [19]. The generated boxes were evaluated by the ground-truth boxes on the training set of WiderFace. We calculated the AP in three IoU thresholds of 0.3, 0.5, and 0.7, so the true positives become gradually harder to reach. The results are shown in Table II, where it can be observed that the proposed LUDA-based method obtains higher AP scores under all the three cases, compared with the GAK-based method, validating the advantage of our LUDA-based pseudo size generation method. Such an advantage also means that we can generate more accurate pseudo bounding boxes at the beginning of training to be beneficial the following processes.

The GAK-based and LUDA-based methods were also compared by yielding bounding boxes on the validation set of WiderFace. The AP scores are shown in the 3rd and 4th entries of Table III, where it can be seen that the accuracy of the generated bounding boxes is extremely low, and especially for the easy subset the AP score is only 7.2%. This observation shows that even though with the ground-truth center points, only applying pseudo size generation methods cannot obtain accurate object sizes.

2) *Effectiveness of the crowdedness-aware loss and the confidence and order-aware refinement scheme:* The crowdedness-aware loss and the confidence and order-aware refinement scheme are the critical components to improve the AP with the point supervision. Based on the pseudo bounding boxes, we trained the detector on the training set of WiderFace with four sittings: 1) using only the crowdedness-aware loss, 2) using only the confidence and order-aware refinement scheme, 3) using neither of the two modules, and 4) using both of the two modules. The AP, MAE, and NMAE results are listed in the 5th to 8th entries of Table III. As listed in the 5th entry of Table III, without the two modules, the AP scores are improved by about 11% on the easy and medium subsets in comparison with the LUDA-based size generation method. However, the values are still low, e.g., 18.6%, 23.4%, and 30.8% AP on the easy, medium, and hard subsets, respectively. This observation demonstrates that it is hard to attain an acceptable detector when trained only with pseudo bounding boxes.

As shown in the 6th and 7th entries of Table III, with the use of the crowdedness-aware loss (resp. the confidence and order-aware refinement scheme), the AP scores increase to 21.3% (easy), 26.8% (medium), and 30.8% (hard) (resp. 55.1% (easy), 55.1% (medium), and 52.5% (hard)), which validate the effectiveness of these two modules. Moreover, it can be known that the refinement module is more effective than the loss. Note that only with the refinement scheme, our approach outperforms PSDDN [7] on the hard subset in the detection task (52.5% AP vs. 39.4% AP) and Shi *et al.* [12] in the counting task (2.3 MAE vs. 3.2 MAE).

Finally, when both modules are activated, our approach achieves the best results in both detection and counting tasks. There is a big jump of AP from using a single module to both modules. The reason is that the crowdedness-aware loss emphasizes the accurate pseudo sizes but neglects to update the noisy sizes during training, while the confidence and

TABLE III: The ablative studies towards the crowdedness-aware loss and the confidence and order-aware refinement scheme, as well as comparisons with state-of-the-art point-supervised detection method [7] and counting method [12] on the validation set of WiderFace [10]. ‘‘C-by-D’’ means counting by detection, and ‘‘C-by-R’’ means counting by regression. ‘‘-’’ means the work does not provide the result. The larger the value of AP is, the better. The lower the values of MAE and NMAE are, the better.

Method	Category	Crowdedness-aware loss	Confidence and order-aware refinement scheme	Detection			Counting	
				easy	medium	hard	MAE	NMAE
PSDDN [7]	C-by-D			60.5	60.5	39.6	-	-
Shi <i>et al.</i> [12]	C-by-R			-	-	-	3.2	0.40
GAK [7]				7.1	12.5	27.3	-	-
LUDA				7.2	12.8	29.5	-	-
Ours	C-by-D			18.6	23.4	30.8	3.4	0.81
		✓		21.3	26.8	35.2	3.6	0.97
			✓	55.1	55.1	52.5	2.3	0.27
		✓	✓	75.8	71.0	64.4	2.2	0.29

TABLE IV: Comparisons with state-of-the-art point-supervised detection methods on the validation set of WiderFace [10]. ‘‘*’’: the AP results are provided by [7]. The larger the value of AP is, the better.

Method	Supervision	easy	medium	hard
Faster R-CNN* [9]	Box	84.0	72.4	34.7
LSC-CNN [8]	Box	57.3	70.1	68.9
CSR-A-thr [8]	Point	30.2	41.9	33.5
PSDNN [7]	Point	60.5	60.5	39.6
LSC-CNN [8]	Point	40.5	62.1	46.2
Ours	Point	75.8	71.0	64.4

order-aware refinement scheme updates the pseudo sizes but it overlooks the importance of the accurate pseudo sizes in the network’s weights updating. The combination of such two modules could well compensates to each other. Numerically, the AP scores of our approach with both two modules increase to 75.8% (easy), 71.0% (medium), and 64.4% (hard). Compared with PSDDN [7], our method improves the AP by more than 10%. The MAE and NMAE of our approach respectively decrease approximately 31.2% and 27.5% against [12]. The results demonstrates the significant superiority of our method in both detection and counting tasks.

Besides, the last row of Table II shows that the refined pseudo sizes improve the AP (0.3) and AP (0.5) by nearly 20%. The gradually enhanced quality of training examples helps the detector become stronger. To demonstrate this improvement, we plot some training examples before and after training on the WiderFace dataset in Fig. 1. Especially for large and sparse objects, the bounding boxes are refined to encompass the face regions.

C. Comparison with State-of-the-Art Methods

1) *Detection*: We compared our approach with state-of-the-art point-supervised detection methods, including PSDDN [7] and LSC-CNN [8], and the recent counting-by-regression method, i.e., CSR-A-thr [8]. The CSR-A-thr is the detection version of CSRNet [11]. Besides, Faster R-CNN [9], a representative box-supervised detector, is also provided as a reference. Table IV shows the AP scores of the above methods on the validation set of WiderFace [10]. From Table IV, we can see that our method outperforms other point-supervised methods to a significant margin (i.e., more than

TABLE V: Comparisons with state-of-the-art counting-by-regression methods (in the top part) and counting-by-detection methods (in the bottom part) on SHA and SHB [19], and WiderFace [10] (WF) datasets. ‘‘-’’: the author does not provide the result. ‘‘*’’: the results are provided by [8]. The lower the values of MAE and RMSE are, the better.

Method	SHA		SHB		WF
	MAE	RMSE	MAE	RMSE	MAE
Zhang <i>et al.</i> [19]	110.2	173.2	26.4	41.3	7.1
CSRNet [11]	68.2	115.0	10.6	16.0	4.3
Cao <i>et al.</i> [28]	67.0	104.5	8.4	13.6	8.5
PSDNN+ [7]	65.9	112.3	9.1	14.2	-
Shi <i>et al.</i> [12]	65.2	109.4	7.2	12.2	3.2
HA-CCN [31]	62.9	94.9	8.1	13.4	-
TinyFace* [41]	237.8	422.8	-	-	-
LC-FCN8 [23]	-	-	13.1	-	-
PSDNN [7]	85.4	159.2	16.1	27.9	-
LSC-CNN [8]	66.4	117.0	8.1	15.7	-
Ours	65.1	104.4	7.8	12.6	2.2

10% AP improvement). Especially for the hard subset, our method increases the AP by 18.2%, compared with LSC-CNN. Even though LSC-CNN (Box) was trained with box annotations, our approach still performs better than it on the easy and medium subsets. In addition, the AP scores of our method are comparable to the box-supervised Faster R-CNN on the easy and medium subsets but better than Faster R-CNN on the hard subset. Here we do not claim that our point-supervised method can reach the performance of box-supervised methods as recent box-supervised methods can achieve above 90% AP on WiderFace. We demonstrate that the point-supervised method is promising, and it is expected that the performance gap between point-supervised methods and the best box-supervised method could be gradually narrowed with more efforts devoted.

2) *Crowd counting*: In addition to detection, we evaluated our method in the crowd counting task. Table V shows the results on SHA and SHB [19], and WiderFace [10] datasets. For a fair comparison, we split the counting methods into two categories: counting-by-regression methods and counting-by-detection methods. Our method achieves the best performance when compared with state-of-the-art counting-by-detection methods. For SHA and SHB, the proposed method is compa-

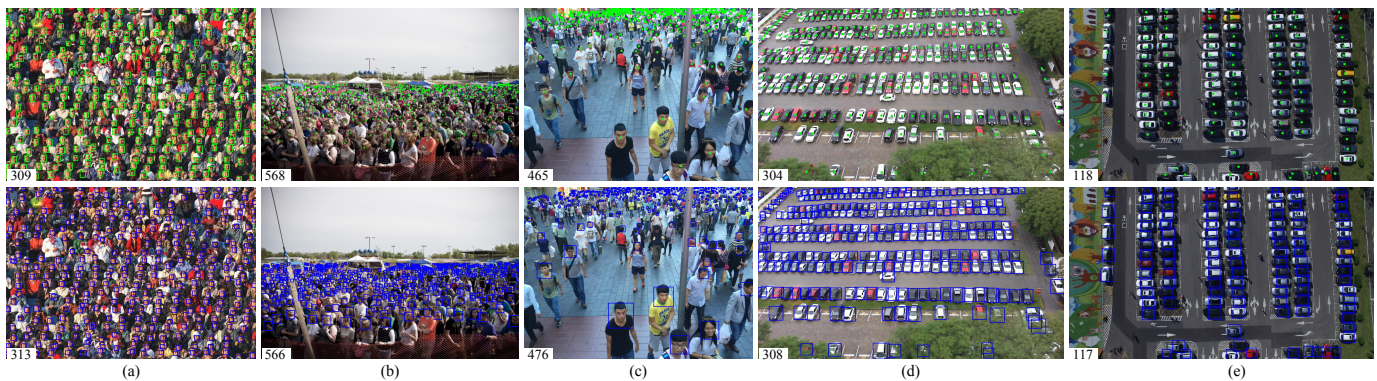


Fig. 3: Qualitative results on (a) WiderFace [10], (b) SHA [19], (c) SHB [19], (d) PUCPR+ [32], and (e) CARPK [32]. The top row shows the ground-truth boxes or points, and counts. The bottom row shows the bounding boxes and counts predicted by our approach. *Zoom in the figure for better viewing.*

TABLE VI: Comparisons of center point localization on SHA and SHB [19] datasets. The larger the value of AP is and the lower the value of MLE is, the better.

Method	SHA		SHB	
	AP (%)	MLE	AP (%)	MLE
PSDDN [7]	73.7	-	75.9	-
CSR-A-thr [8]	-	16.8	-	12.3
LSC-CNN [8]	67.6	9.6	76.0	9.0
Ours	85.3	8.0	91.6	6.0

able to state-of-the-art counting-by-regression methods, such as Shi *et al.* [12] and HA-CCN [31].

Note that our method not only provides the count but also estimates the bounding boxes for object instances. We also qualitatively evaluated the proposed method by visualizing the predicted bounding boxes on the WiderFace, SHA, and SHB datasets in Fig. 3. Besides, Fig. 4 compares the predicted boxes by our method with the estimated density maps by counting-by-regression methods on the SHA and SHB datasets. We argue that the box outputs of our method are more meaningful than the density maps of counting-by-regression methods because the boxes provide high-level understanding in crowds.

3) *Center point localization*: To evaluate the localization ability for the datasets with point-level annotations, we compared our method with PSDNN [7], CSR-A-thr [8], and LSC-CNN [8] on the SHA and SHB [19] datasets. Table VI presents the results of the AP and MLE metrics. Our approach obtains the best results, showing 85.3% AP and 8.0 MLE for SHA, and 91.6% AP and 6.0 MLE for SHB.

4) *Counting from drone view*: To evaluate the generalization ability in other domains, we trained our model on the CARPK and PUCPR+ benchmarks [32]. The benchmarks provide densely-packed car counting images from drone view. Table VII reports the MAE and RMSE results of our method and state-of-the-art vehicle counting methods in [20], [22], [32]–[34]. The results show that our method consistently performs better than these methods. This demonstrates that our model is flexible for various detection and counting tasks. Some qualitative results on CARPK and PUCPR+ are shown in Fig. 3.

TABLE VII: Comparisons with state-of-the-art vehicle counting methods on the CARPK and PUCPR+ benchmarks [32]. The lower the values of MAE and RMSE are, the better.

Method	CARPK		PUCPR+	
	MAE	RMSE	MAE	RMSE
LPN Counting [32]	23.80	36.79	22.76	34.46
RetinaNet [20]	16.62	22.30	24.58	33.12
IEP Counting [33]	51.83	-	15.17	-
Goldman <i>et al.</i> [22]	6.77	8.52	7.16	12.00
Li <i>et al.</i> [34]	5.24	7.38	3.92	5.06
Ours	4.95	7.09	3.20	4.83

V. CONCLUSION

In this paper, we have presented a self-training approach to train a typical detector with only point-level annotations such that the detector can accurately detect and count objects in crowd scenes. This is achieved by the proposed locally-uniform distribution assumption, the crowdedness-aware loss, the confidence and order-aware refinement scheme, and the effective decoding method, which promote the detector to generate accurate bounding boxes in a coarse-to-fine and end-to-end manner. Extensive experimental results have demonstrated that the proposed approach achieves the best performance in point-supervised detection and counting tasks among detection-based methods, and our method can achieve comparable performance to state-of-the-art counting-by-regression methods. We believe that DNN-based object detection in crowds with only point supervision is a potential and promising research issue.

REFERENCES

- [1] V. A. Sindagi and V. M. Patel, “A survey of recent advances in cnn-based single image crowd counting and density estimation,” *Pattern Recognition Letters*, vol. 107, pp. 3–16, 2018.
- [2] T. Li, H. Chang, M. Wang, B. Ni, R. Hong, and S. Yan, “Crowded scene analysis: A survey,” *IEEE Trans. Circuits Syst. Video Technol.*, vol. 25, no. 3, pp. 367–386, 2015.
- [3] D. Kang, Z. Ma, and A. B. Chan, “Beyond counting: comparisons of density maps for crowd analysis tasks-counting, detection, and tracking,” *IEEE Trans. Circuits Syst. Video Technol.*, vol. 29, no. 5, pp. 1408–1422, 2019.
- [4] A. B. Chan, Z.-S. J. Liang, and N. Vasconcelos, “Privacy preserving crowd monitoring: Counting people without people models or tracking,” in *CVPR*. IEEE, 2008, pp. 1–7.

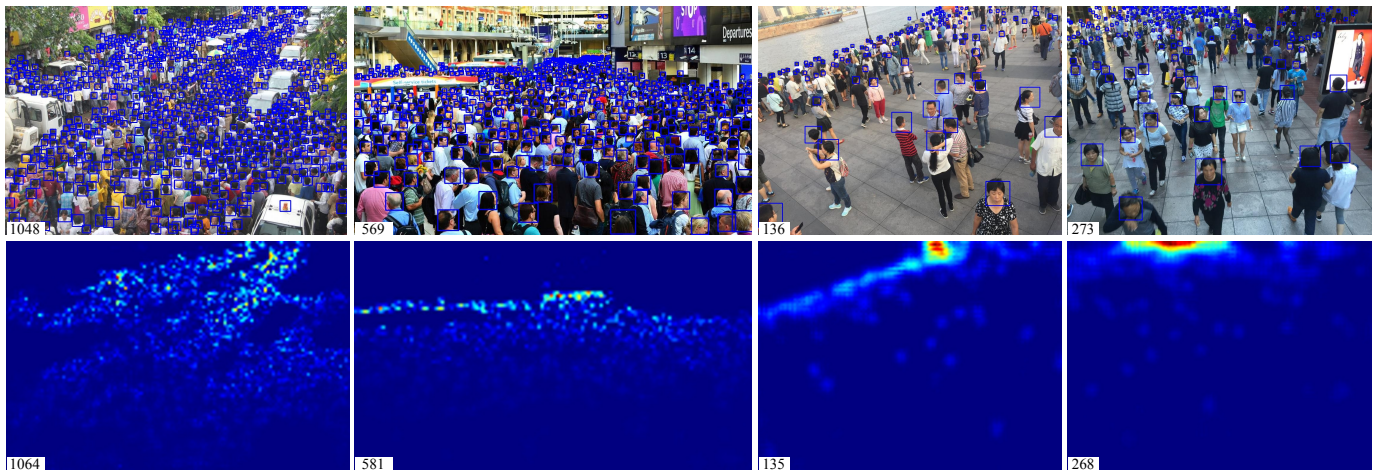


Fig. 4: Comparisons between the bounding boxes (at top row) produced by our approach and the density maps (at bottom row) produced by CSRNet [11] on the SHA and SHB [19] datasets. The predicted counts are placed at the bottom-left corner of an image. The ground-truth counts from left to right images are 1068, 584, 139, and 274. *Zoom in the figure for better viewing.*

- [5] Y.-L. Chen, B.-F. Wu, H.-Y. Huang, and C.-J. Fan, "A real-time vision system for nighttime vehicle detection and traffic surveillance," *IEEE Trans. Ind. Electron.*, vol. 58, no. 5, pp. 2030–2044, 2011.
- [6] Z.-Q. Zhao, P. Zheng, S.-t. Xu, and X. Wu, "Object detection with deep learning: a review," *IEEE Trans. Neural Netw. Learn. Syst.*, 2019.
- [7] Y. Liu, M. Shi, Q. Zhao, and X. Wang, "Point in, box out: Beyond counting persons in crowds," in *CVPR*, 2019, pp. 6469–6478.
- [8] D. B. Sam, S. V. Peri, M. Narayanan Sundararaman, A. Kamath, and R. V. Babu, "Locate, size and count: Accurately resolving people in dense crowds via detection," *IEEE Trans. Pattern Anal. Mach. Intell.*, 2020.
- [9] S. Ren, K. He, R. Girshick, and J. Sun, "Faster r-cnn: Towards real-time object detection with region proposal networks," in *Advances in neural information processing systems*, 2015, pp. 91–99.
- [10] S. Yang, P. Luo, C.-C. Loy, and X. Tang, "Wider face: A face detection benchmark," in *CVPR*, 2016, pp. 5525–5533.
- [11] Y. Li, X. Zhang, and D. Chen, "Csrnet: Dilated convolutional neural networks for understanding the highly congested scenes," in *CVPR*. IEEE, 2018, pp. 1091–1100.
- [12] Z. Shi, P. Mettes, and C. G. Snoek, "Counting with focus for free," *ICCV*, 2019.
- [13] G. Gao, J. Gao, Q. Liu, Q. Wang, and Y. Wang, "Cnn-based density estimation and crowd counting: A survey," *arXiv preprint arXiv:2003.12783*, 2020.
- [14] M. Rodríguez, I. Laptev, J. Sivic, and J.-Y. Audibert, "Density-aware person detection and tracking in crowds," in *ICCV*. IEEE, 2011, pp. 2423–2430.
- [15] Y. Xiang, A. Alahi, and S. Savarese, "Learning to track: Online multi-object tracking by decision making," in *ICCV*, 2015, pp. 4705–4713.
- [16] M. A. Turk and A. P. Pentland, "Face recognition using eigenfaces," in *CVPR*. IEEE, 1991, pp. 586–591.
- [17] W. Li, R. Zhao, T. Xiao, and X. Wang, "Deepreid: Deep filter pairing neural network for person re-identification," in *CVPR*, 2014, pp. 152–159.
- [18] W. Liu, S. Liao, W. Ren, W. Hu, and Y. Yu, "High-level semantic feature detection: A new perspective for pedestrian detection," in *CVPR*, June 2019, pp. 5187–5196.
- [19] Y. Zhang, D. Zhou, S. Chen, S. Gao, and Y. Ma, "Single-image crowd counting via multi-column convolutional neural network," in *CVPR*. IEEE, 2016, pp. 589–597.
- [20] T.-Y. Lin, P. Goyal, R. Girshick, K. He, and P. Dollár, "Focal loss for dense object detection," in *ICCV*, Oct 2017, pp. 2980–2988.
- [21] X. Zhou, D. Wang, and P. Krähenbühl, "Objects as points," *arXiv preprint arXiv:1904.07850*, 2019.
- [22] E. Goldman, R. Herzig, A. Eisenschadt, J. Goldberger, and T. Hassner, "Precise detection in densely packed scenes," in *CVPR*, 2019, pp. 5227–5236.
- [23] I. H. Laradji, N. Rostamzadeh, P. O. Pinheiro, D. Vazquez, and M. Schmidt, "Where are the blobs: Counting by localization with point supervision," in *ECCV*, 2018, pp. 547–562.
- [24] H. Idrees, M. Tayyab, K. Athrey, D. Zhang, S. Al-Maadeed, N. Rajpoot, and M. Shah, "Composition loss for counting, density map estimation and localization in dense crowds," in *ECCV*, 2018, pp. 532–546.
- [25] C. Zhang, H. Li, X. Wang, and X. Yang, "Cross-scene crowd counting via deep convolutional neural networks," in *CVPR*. IEEE, 2015, pp. 833–841.
- [26] Y. Wang, J. Hou, and L.-P. Chau, "Object counting in video surveillance using multi-scale density map regression," in *ICASSP*. IEEE, 2019, pp. 2422–2426.
- [27] A. B. Chan and N. Vasconcelos, "Bayesian poisson regression for crowd counting," in *ICCV*. IEEE, 2009, pp. 545–551.
- [28] X. Cao, Z. Wang, Y. Zhao, and F. Su, "Scale aggregation network for accurate and efficient crowd counting," in *ECCV*, 2018, pp. 734–750.
- [29] V. Lempitsky and A. Zisserman, "Learning to count objects in images," in *NIPS*, 2010, pp. 1324–1332.
- [30] K. Simonyan and A. Zisserman, "Very deep convolutional networks for large-scale image recognition," in *ICLR*, 2014.
- [31] V. A. Sindagi and V. M. Patel, "Ha-ccn: Hierarchical attention-based crowd counting network," *IEEE Transactions on Image Processing*, vol. 29, pp. 323–335, 2019.
- [32] M.-R. Hsieh, Y.-L. Lin, and W. H. Hsu, "Drone-based object counting by spatially regularized regional proposal network," in *ICCV*, 2017, pp. 4145–4153.
- [33] T. Stahl, S. L. Pinteá, and J. C. van Gemert, "Divide and count: Generic object counting by image divisions," *IEEE Trans. Image Process.*, vol. 28, no. 2, pp. 1035–1044, 2018.
- [34] W. Li, H. Li, Q. Wu, X. Chen, and K. N. Ngan, "Simultaneously detecting and counting dense vehicles from drone images," *IEEE Transactions on Industrial Electronics*, vol. 66, no. 12, pp. 9651–9662, 2019.
- [35] K. He, X. Zhang, S. Ren, and J. Sun, "Deep residual learning for image recognition," in *CVPR*, 2016, pp. 770–778.
- [36] R. Girshick, "Fast r-cnn," in *ICCV*. IEEE, Dec 2015, pp. 1440–1448.
- [37] A. Shrivastava, A. Gupta, and R. Girshick, "Training region-based object detectors with online hard example mining," in *CVPR*, 2016, pp. 761–769.
- [38] A. RoyChowdhury, P. Chakrabarty, A. Singh, S. Jin, H. Jiang, L. Cao, and E. Learned-Miller, "Automatic adaptation of object detectors to new domains using self-training," in *CVPR*, 2019, pp. 780–790.
- [39] A. Krizhevsky, I. Sutskever, and G. E. Hinton, "Imagenet classification with deep convolutional neural networks," in *NIPS*, 2012, pp. 1097–1105.
- [40] D. P. Kingma and J. Ba, "Adam: A method for stochastic optimization," *arXiv preprint arXiv:1412.6980*, 2014.
- [41] P. Hu and D. Ramanan, "Finding tiny faces," in *CVPR*, 2017, pp. 951–959.